Effect of the vertical component of diffusion on passive scalar transport in an isolated vortex model

Konstantin V. Koshel*
V. I. Il'ichev Pacific Oceanological Institute of RAS, 43, Baltiyskaya Street, Vladivostok 690041, Russia and Far Eastern Federal University, 8, Sukhanova Street, Vladivostok 690950, Russia

Evgeny A. Ryzhov†
V. I. Il'ichev Pacific Oceanological Institute of RAS, 43, Baltiyskaya Street, Vladivostok 690041, Russia

Vladimir V. Zhmur‡
P. P. Shirshov Institute of Oceanology of RAS, 36, Nakhimovski prospect, Moscow 117997, Russia and Moscow Institute of Physics and Technology, 9, Institutskiy Pereulok, Dolgoprudnyi, Moscow region 141700, Russia

(Received 4 June 2015; revised manuscript received 8 September 2015; published 30 November 2015)

On the basis of the ellipsoidal vortex model and a Monte-Carlo-type diffusion simulation, we examine the flux and ensuing distribution of passive fluid particles through the boundary of an idealized geophysical vortex. Our focus is on features that the horizontal and vertical diffusion components introduce into the fluid particle transport. We examine the concurrent effect of both components, and we compare it with the only horizontal diffusion impact. We analyze the ellipsoid vortex model in two cases: (i) the steady state when the ellipsoid is motionless, i.e., there is no variation in its axes' lengths, and consequently the exterior fluid is not being stirred; (ii) the perturbed case when the ellipsoid rotates periodically, varying it axes' lengths, which results in the appearance of stirred fluid outside the ellipsoid. Influenced by diffusion, a fluid particle is now permitted to move to another vertical horizon, thus there is an increased possibility that the particle will eventually be located in the exterior stirred region rather than in the ellipsoid vortex with the regular dynamics. This is because the area of the horizontal section of the ellipsoid vortex decreases with depth, but the region of stirred exterior fluid extends significantly deeper. Numerical calculations show that factoring in the vertical component of diffusion significantly affects scalar spreading in the horizontal plane in the perturbed case, while in the steady state the vertical component of diffusion only induces dispersion linear growth according to a Gaussian distribution.

DOI: 10.1103/PhysRevE.92.053021 PACS number(s): 47.10.Df, 47.27.De, 47.32.cd

I. INTRODUCTION

Isolated vortices evolving in a sheared environment are often modeled by the ellipsoidal vortex model [1–3]. This model is a generalization of the planar Kida vortex model [4] in that it accounts for a linear distribution of the buoyancy frequency. Hence, the ellipsoidal vortex model is considered to be more suitable to look into the dynamics of ocean vortices. The model has been studied intensely over the past 30 years [1–3,5–9]. However, the recent review [10] on the ellipsoidal vortex model evidences that there is still sizable interest among researchers. Part of this interest comes from the simplicity of the model, whose dynamics reduces to a set of ordinary differential equations that govern the evolution of the ellipsoid's horizontal axes and orientation, and a passive scalar inside the vortex and in its vicinity. On the other hand, the model offers interesting effects from the standpoint of nonlinear dynamics, and it can also be used to characterize a vast range of phenomena that are intrinsic to the real geophysical vortices evolving in complex background flows.

The model is based on fluid particles inside a vortex that always move regularly, with their trajectories coinciding with the streamlines of the fixed vortex. However, for fluid particles outside the vortex, that holds true only if the vortex does not change its form, thus generating a stationary velocity field. When moving periodically, the vortex perturbs neighboring fluid, inducing fluid particles, to diverge exponentially. This exponential divergence is usually called chaotic advection [11–13] in hydrodynamics applications, and it is the cause of effective stirring. Depending on the initial sizes of the ellipsoid's axes and its alignment relative to the external strain, the ellipsoid is known to be able to oscillate, rotate slightly (changing the lengths of its axes), and elongate infinitely. The first two regimes are periodic and thus can result in chaotic advection [9] (analogous effects are well known in the case of a plane Kida vortex [14–16]).

A significant restriction of the model is that there is no flux of fluid particles through the vortex's boundary. The boundary serves as a barrier ensuring a nonzero vorticity gradient, and as a result fluid particles are prevented from crossing the boundary due to chaotic advection [17]. In this case, the boundary plays the role of an impenetrable barrier. Such barriers are unlikely to be observed in nature as most barriers, in fact, are penetrable and vary in time and space. A large body of literature is devoted to studying transport barriers that occur in the ocean and atmosphere [18–24]. However, these studies mostly examine real complex velocity fields that do not allow one to single out the effects of advection or diffusion separately. Therefore, one needs to employ simplified models to get insights into the influence of advection and diffusion separately.

It is of interest how the interior of the vortex, which often consists of fluid with sufficiently different features (such as salinity or temperature), can permeate through the boundary

*kvkoshel@poi.dvo.ru
†ryzhovea@poi.dvo.ru
‡zhmur@hotmail.com

and spread in the exterior flow. One way to overcome the ellipsoidal vortex model's restriction on inhibiting fluid particle transport across the boundary was introduced in Ref. [25]. A low-scale diffusion process was imposed, thus allowing fluid particles to jump through the boundary. In this paper, only horizontal diffusion was considered, as the main goal was to examine the difference between the steady state with the ellipsoid not changing the lengths of its axes, and the perturbed state with the rotating ellipsoid. The present paper generalizes and extends the results of the previous one in that it incorporates the vertical component of diffusion, which permits fluid particles to jump between vertical horizons. Therefore, the phenomenon of chaotic advection facilitating diffusion-induced transport [26–30] must be taken into account.

Without diffusion, the model does not allow any vertical motion; fluid particles always move at the same horizon, i.e., where they originated. The main idea of the present work is that enabling fluid particles to jump between horizons may increase the flux through the vortex's boundary and consequently result in a peculiar passive scalar distribution.

We investigate the influence of the vertical component of diffusion on the transport of passive scalars through the boundary of the ellipsoid vortex evolving in a linear shear flow. The cooperative impact of the horizontal and vertical components of diffusion is in question. The vertical and horizontal components are considered to be proportional as follows. As with the ellipsoid model, there is a normalizing factor between the vertical and horizontal length scales. Provided N is the buoyancy frequency and f is the Coriolis parameter, the horizontal scale is larger than the vertical one by N/f, which we further take as 20, which is characteristic to the middle latitudes, whereas the vertical diffusivity is at the very least one order smaller than the horizontal one [31,32] (depending on a region and assumptions, this relation may span from 10^{-6} up to 10^{-1}). Hence, we exploit the following normalized vertical diffusivity: $\kappa_z = 10^{-1}\frac{N}{f}\kappa = 2\kappa$, where κ is the horizontal diffusivity. In other words, despite being some orders of magnitude smaller, vertical diffusion causes fluid particles to cover, normalized by the vertical ellipsoid scale, distances in the vertical plane that are comparable to the horizontal ones, normalized by the ellipsoid's horizontal scale. In the end, the chances for a fluid particle to permeate through the ellipsoid's boundary in the horizontal direction or in the vertical one are thus comparable.

II. THE ELLIPSOIDAL VORTEX MODEL IN STEADY AND PERTURBED STATES

We outline the ellipsoidal vortex model and the governing equations used (see [1,3,9] for a detailed derivation). Given the quasigeostrophic approximation on the f plane, a constant buoyancy frequency, $N = \text{const}$, and an inviscid and incompressible flow occupying a semi-infinite space, an ellipsoid form varies in time and space induced by a linear shear in accordance with the governing equations,

$$\begin{aligned} \frac{da}{dt} &= ae\cos(2\theta), \quad \frac{db}{dt} = -be\cos(2\theta), \\ \frac{d\theta}{dt} &= \Omega + \gamma - \frac{a^2+b^2}{a^2-b^2}e\sin(2\theta), \end{aligned} \tag{1}$$

where a,b are the horizontal semiaxes, θ is the ellipsoid orientation against the shear flow, γ is the exterior vorticity, e is the exterior shear, and

$$\Omega = (\alpha-\gamma)ab\tilde{c}\int_0^\infty \frac{\mu d\mu}{(a^2+\mu)(b^2+\mu)\sqrt{\delta(\mu)}}. \tag{2}$$

$\delta(\mu) = (a^2+\mu)+(b^2+\mu)+(\tilde{c}^2+\mu)$, $f = \text{const}$ is the Coriolis parameter, and $\alpha = \text{const} \neq 0$ is the vorticity inside the ellipsoid. The parameter $\tilde{c} = c\,N/f$ is proportional to the ellipsoid's vertical axis c, which does not vary in time.

The velocity field generated by the varying ellipsoid form ensues from the equations

$$\begin{aligned} u &= ex - \gamma y + \tilde{u}\cos\theta - \tilde{v}\sin\theta, \\ v &= \gamma x - ey + \tilde{u}\sin\theta + \tilde{v}\cos\theta, \end{aligned} \tag{3}$$

where the first two terms in both equations are the external flow, and the last two indicate the ellipsoid influence as follows:

$$\begin{aligned} \tilde{u} &= -(\alpha-\gamma)\int_\lambda^\infty \frac{\tilde{y}d\mu}{(b^2+\mu)\sqrt{\delta(\mu)}}, \\ \tilde{v} &= (\alpha-\gamma)\int_\lambda^\infty \frac{\tilde{x}d\mu}{(a^2+\mu)\sqrt{\delta(\mu)}}. \end{aligned} \tag{4}$$

Here, $\tilde{x} = x\cos\theta + y\sin\theta$, $\tilde{y} = -x\sin\theta + y\cos\theta$, and λ is equal to zero inside the ellipsoid, or it should be taken as a positive root of the equation $\frac{\tilde{x}^2}{a^2+\lambda} + \frac{\tilde{y}^2}{b^2+\lambda} + \frac{(z)^2}{\tilde{c}^2+\lambda} = 1$. It should be emphasized that z determines a horizon at which the motion realizes, as $z = 0$ corresponds to the surface.

Solving jointly Eqs. (1) and (3), one arrives at trajectories of fluid particles affected by the ellipsoid changing its form due to a linear shear. Hereafter, we use the values $e = 0.1$, $\gamma = 0$, and $\tilde{c} = 1$. There are parameters that ensure that the ellipsoid remains stationary, thus creating a stationary velocity field (3). Given our choice of values, the stationary configuration is as $\frac{a(0)}{b(0)} = 1.0551$, $\theta(0) = \frac{\pi}{4}$. Figure 1(a) depicts the streamline structure at the surface, showing the induced region encompassed by a separatrix (the bold line), where fluid particles move periodically around the ellipsoid. The dashed line is the separatrix at depth $z = 1.5$ indicating that the closed recirculation zone area decreases with depth slower than the ellipsoid horizontal section area (the ellipsoid reaches a depth $z = 1$).

Given the different initial values of the parameters, the ellipsoid starts moving when its horizontal axes vary according to Eq. (1). This variation induces a perturbation to fluid particle trajectories leading to exponential divergence of initially close trajectories [33,34]. Figure 1(b) illustrates the exponential divergence of trajectories [the initial positions are plotted in Fig. 2(a)]. One of the trajectories starts in the regular dynamics island, thus moving in a quasiperiodic way. The other originates in the chaotic sea, completes a few rotations about the ellipsoid, and eventually escapes to the exterior flow through the chaotic region established instead of the broken steady-state separatrix. Actually, a trajectory originating in the chaotic region may complete a very large number of revolutions about the ellipsoid, but eventually it always escapes to the exterior region.

Figure 2 demonstrates Poincaré sections plotted in a period of the ellipsoid oscillation at the surface, $z = 0$ [Fig. 2(a)], and

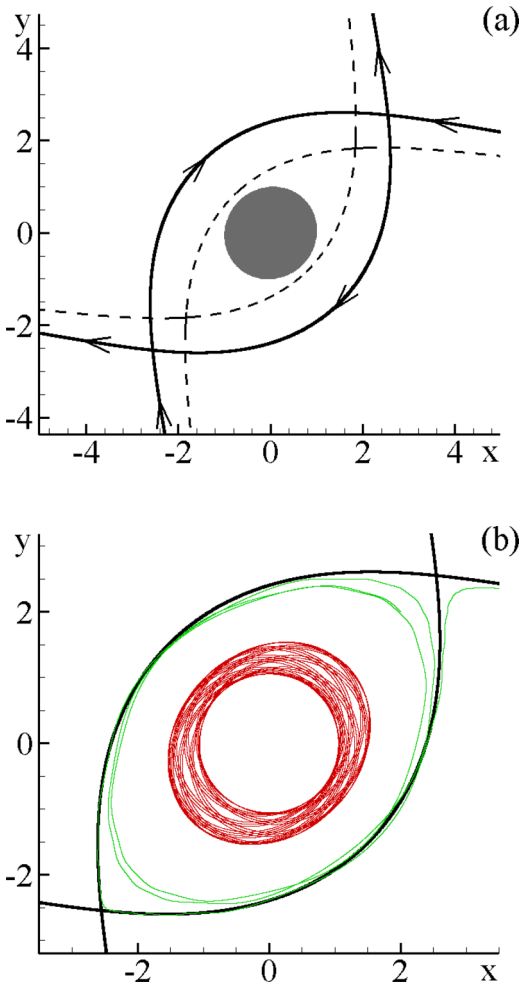

FIG. 1. (Color online) (a) The steady-state streamline structure. The filled central region is the stationary ellipsoid horizontal section at $z = 0$. The bold line is a separatrix demarcating the closed recirculation region from the exterior flow at $z = 0$. The dashed line indicates the separatrix at depth $z = 1.5$. (b) Two trajectories of the perturbed system. One quasiperiodic regular trajectory always stays near the ellipsoid. The second one is irregular completing a few revolutions about the core and then escapes to the exterior flow.

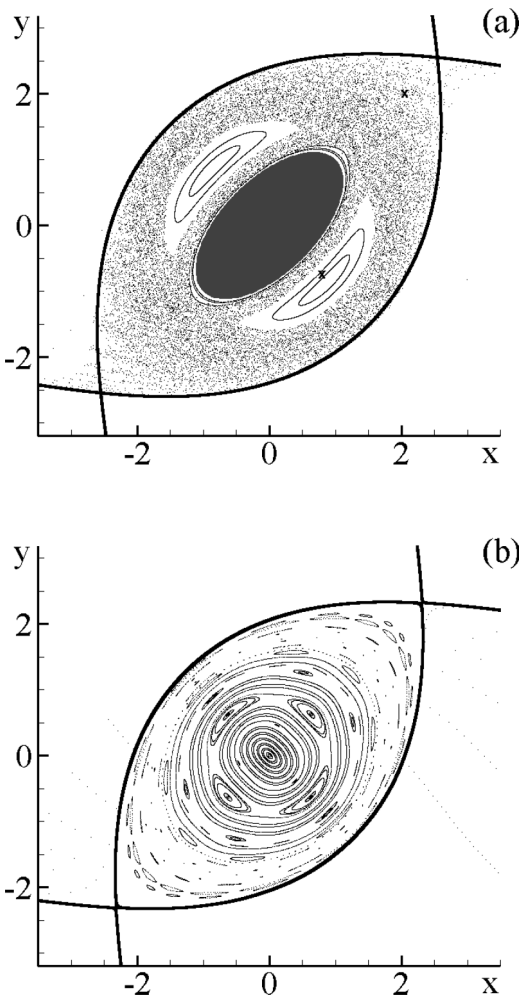

FIG. 2. Poincaré sections of the perturbed state as the ellipsoid rotates varying its horizontal axes. (a) $z = 0$, (b) $z = 1.5$. The bold curves correspond to the steady-state separatrices shown in Fig. 1(a). The crosses mark the initial positions of the trajectories plotted in Fig. 1(b).

at the horizon, $z = 1.5$ [Fig. 2(b)]. These two sections indicate that the structure of the Poincaré sections varies significantly at different horizons. This occurs because the perturbation introduced by the ellipsoid rotation also changes with depth. Thereby, there are different perturbation magnitudes (however, the frequencies stay the same since they are always equal to the frequency of the ellipsoid's one full rotation) at different horizons. Despite being strikingly different at relatively distant horizons, the structure of the Poincaré sections changes continuously, as evidenced from Fig. 3. The figure depicts three Poincaré sections at close horizons; Figs. 3(a), 3(b), and 3(c) correspond to the horizons $z = 0.95$, 1, and 1.05, respectively.

III. IMPOSING DIFFUSION PROCESSES

To model turbulent diffusion, we use the following Monte Carlo procedure [35–38]: Let us assume that the passive scalar concentration described by a function $q(\mathbf{r},t)$ is subjected to a random velocity field $\mathbf{U}(\mathbf{r},t)$. Hence,

$$\left(\frac{\partial}{\partial t} + \mathbf{U}(\mathbf{r},t)\frac{\partial}{\partial \mathbf{r}}\right)q(\mathbf{r},t) = \kappa\frac{\partial^2}{\partial \mathbf{r}^2}q(\mathbf{r},t),$$
$$q(\mathbf{r},0) = q_0(\mathbf{r}), \tag{5}$$

where κ is the diffusivity. Now, one can introduce a scalar field $\tilde{q}(\mathbf{r})$ complying with the equation

$$\left(\frac{\partial}{\partial t} + \mathbf{U}(\mathbf{r},t)\frac{\partial}{\partial \mathbf{r}}\right)\tilde{q}(\mathbf{r},t) = -\boldsymbol{\alpha}(t)\frac{\partial}{\partial \mathbf{r}}\tilde{q}(\mathbf{r},t),$$
$$\tilde{q}(\mathbf{r},0) = q_0(\mathbf{r}), \tag{6}$$

where $\boldsymbol{\alpha}(t)$ is a δ-correlated Gaussian process such as $\langle\boldsymbol{\alpha}(t)\rangle = \mathbf{0}, \langle\alpha_i(t)\alpha_j(t')\rangle = 2\kappa\delta_{ij}\delta(t-t')$, $i,j = 1,2$; $\langle\alpha_3(t)\alpha_j(t')\rangle = 2\kappa_z\delta_{3j}\delta(t-t')$, $j = 1,2,3$; and δ_{ij} is the Kronecker delta, $\delta(t)$ is the Dirac function, and t, t' are two instants in time. Taking advantage of the introduced function, one arrives at the averaged solution [35]

$$q(\mathbf{r},t) = \langle\tilde{q}(\mathbf{r},t)\rangle_{\boldsymbol{\alpha}}. \tag{7}$$

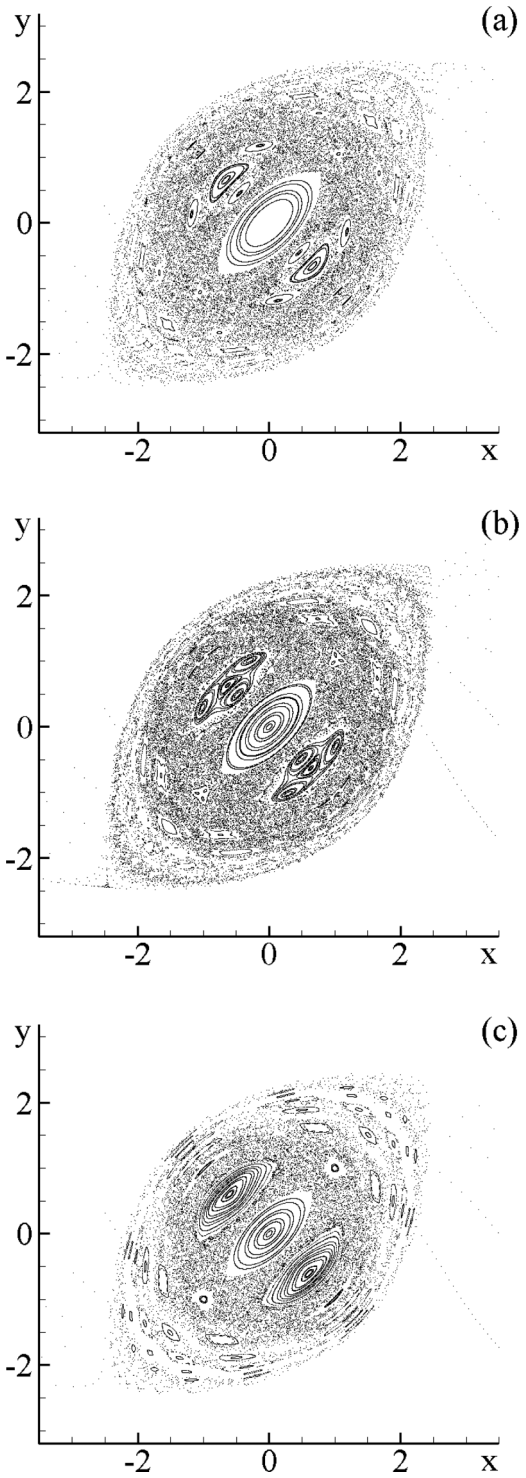

FIG. 3. Continuous change in the Poincaré section structure at near vertical horizons. (a) $z = 0.95$, (b) $z = \tilde{c} = 1$, the limiting point of the ellipsoid in the vertical direction, and (c) $z = 1.05$.

The random process $\boldsymbol{\alpha}(t)$ featured in Eq. (6) is the modeled diffusion process depending on the time scale and diffusivity $\boldsymbol{\kappa}$.

Eventually, the equations governing a fluid particle trajectory subjected to the ellipsoid motion and diffusion impact ensue from (3) as

$$\begin{aligned} u &= ex - \gamma y + \tilde{u}\cos\theta - \tilde{v}\sin\theta + \alpha_x, \\ v &= \gamma x - ey + \tilde{u}\sin\theta + \tilde{v}\cos\theta + \alpha_y, \\ w &= \alpha_z, \end{aligned} \tag{8}$$

where the α_x,α_y terms correspond to the horizontal diffusivity κ, and α_z complies with the vertical diffusivity κ_z.

IV. MARKER DISPERSION DUE TO DIFFUSION

In this section, we look into how passive scalars move subjected to the simultaneous effect of chaotic advection and diffusion. We distribute $\sim 6 \times 10^3$ scalars inside the ellipsoid, as there are seven layers inside the ellipsoid with evenly distributed scalars in every layer. Then, we follow scalar distributions for $\sim$20 ellipsoid revolutions as both horizontal and vertical components of diffusion are at work. We carry out the same routine for 6×10^3 realizations of the random process $\boldsymbol{\alpha}(t)$ in order to smooth the resulting scalar distributions due to assumed averaging. Finally, we compare these results with the ones obtained in the case of only horizontal diffusion [25] to single out the impact of the diffusion vertical component.

To start, we address the steady state, as the ellipsoid stays undeformed. This state is illustrated in Fig. 1(a) as $a(0)/b(0) = 1.0551$, $\theta(0) = \pi/4$. The ellipsoid axes remain unchanged, hence there is no perturbation to exterior fluid particles. Then, when the diffusion is imposed, fluid particles are now able to redirect their paths from one streamline to some other. Therefore, the fluid particles tend to be redistributed in space in accord with a Gaussian distribution.

Figure 4 clarifies the latter observation. The initial concentration field of passive scalars within the ellipsoid is equal to the number of realizations 6×10^3. Figure 4 shows the concentration field after 40 dimensionless time intervals as the horizontal diffusion component is $\kappa = 0.01$ and the vertical component is $\kappa_z = 2\kappa$. Figure 4(a) corresponds to the surface layer at $z = 0$, while Fig. 4(b) corresponds to the layer comprising the bottom tip of the ellipsoid at $z = \tilde{c} = 1$. The figures indicate that, because of the vertical component of diffusion, the maximal value of the scalar concentration field varies in space. A higher concentration is observed outside the ellipsoid [Fig. 4(b)] in comparison with the surface concentration inside the ellipsoid [Fig. 4(a)].

Figures 4(c) and 4(d) show an analogous scalar concentration field but without the diffusion vertical component $\kappa_z = 0$. This configuration was previously investigated in Ref. [25]. Figure 4(c) corresponds to the surface layer $z = 0$, while Fig. 4(d) shows the concentration field in the layer comprising the bottom tip of the ellipsoid. Since scalars are now able to move only in the horizontal plane, the concentration is much higher at the surface due to a significantly larger number of initial scalars (1150) compared to a smaller number in the layer comprising the ellipsoid bottom tip (216).

Now, we look into the dynamics of the perturbed state as the ellipsoid changes its form and orientation in time. Because of the varying lengths of the horizontal axes, a,b, the ellipsoid stirs the neighboring fluid by periodically perturbing it, thus causing exponential divergence of initially close fluid trajectories. This state is illustrated in Fig. 2 as $a(0)/b(0) = 2$,

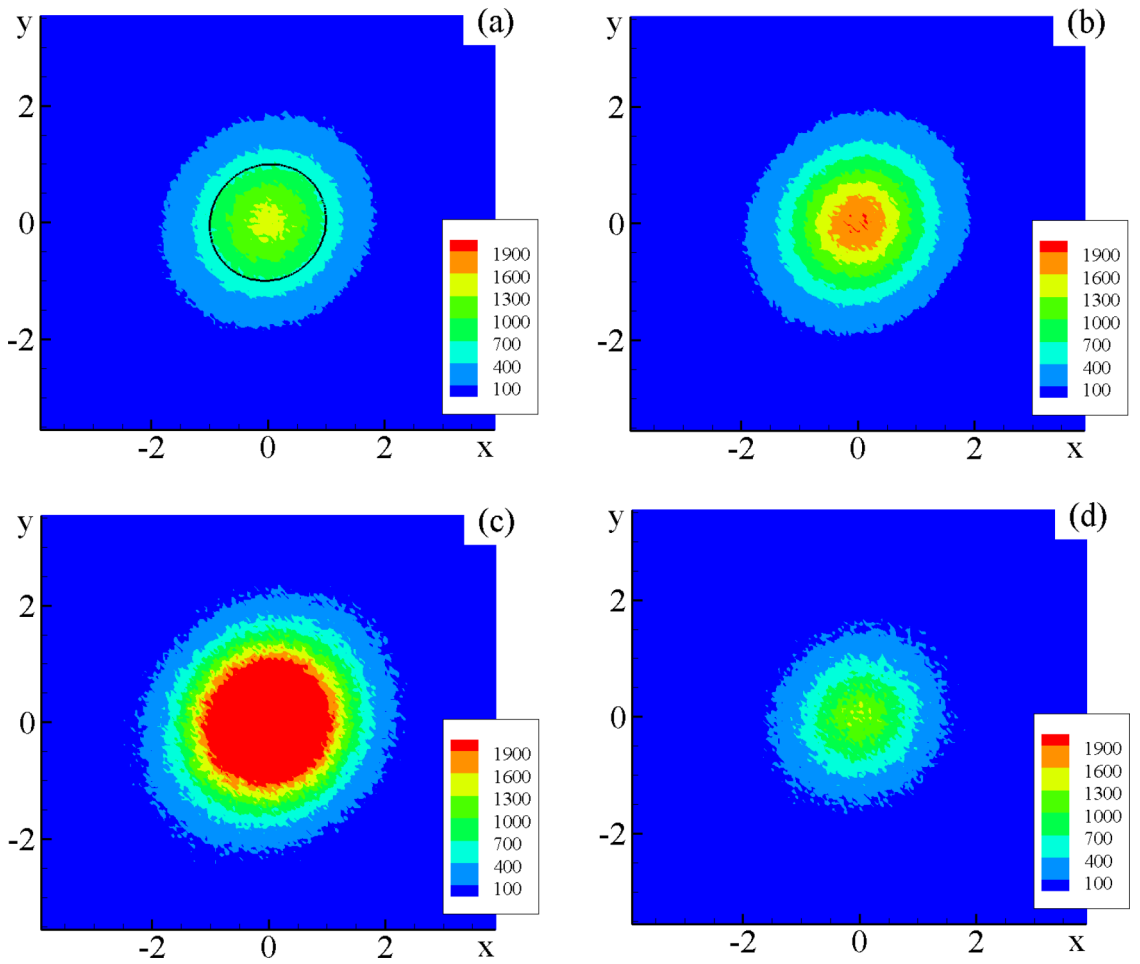

FIG. 4. (Color online) The steady state as $a(0)/b(0) = 1.0551, \theta(0) = \pi/4$. Passive scalar distributions after 40 dimensionless time intervals from the initial concentration of 6×10^3 in each node as the diffusion horizontal component is $\kappa = 0.01$. (a) $\kappa_z = 2\kappa$—the surface layer $z = 0$, the bold curve marks the steady ellipsoid boundary; (b) $\kappa_z = 2\kappa$—the layer comprising the bottom tip of the ellipsoid, $z = \tilde{c} = 1$; (c),(d) the same as in (a),(b), respectively, except that there is no vertical diffusion $\kappa_z = 0$.

$\theta(0) = \pi/4$. As the ellipsoid rotates, the phase space shrinks and elongates periodically. Therefore, to analyze the system evolution in time, one needs to consider passive scalar positions only at the moments when the ellipsoid takes on its original form and orientation. The ellipsoid completes a full rotation and returns to its initial state in a time interval $T_r = 1.891\,65$. Hence, 40 time intervals equal $21T_r$. Figure 5 illustrates the concentration field after this time interval. The sequence of the figures is the same as in Fig. 4.

As indicated by the figures, the perturbed state ensures an enhanced dispersion of the concentration field because along with the diffusion transport there occurs chaotic advection facilitating the trajectory spreading. Analogously to the steady state, the concentration field maximum shifts in the vertical direction.

V. SCALAR PROBABILITY DENSITY AND DISPERSION

Now, we analyze in detail how the concentration fields evolve in time and space. As a numerical estimate, we make use of the following probability density. We single out nested ellipsoidal rings of equal volume with the same ellipticity (1.0551 in the steady state, 2 in the perturbed state), and we calculate the number of scalars that get into some of the ellipsoidal rings. As a result, we construct a probability density identifying the scalar concentration change in space. A discrete analog of a probability density in our case reads

$$p = \frac{N_{\Delta V}}{N}, \tag{9}$$

where $N_{\Delta V}$ is the number of scalars inside an ellipsoidal ring of a volume ΔV, and N is the total number of scalars encompassed in the total volume V. Scaling of quantity (9) depends on the volume ΔV, but it does not impact the shape of the probability curves, so it was not taken into account. We choose a rather fine difference ΔV that allows us to observe sought-after effects. The only result that occurs from changing ΔV is that the curves will be elongated or shrunk along the ordinate axis, but significant features will remain. Therefore, initially we have $p = 0.2$ inside the ellipsoid, since we choose ΔV equal to $1/5$ of the initial volume, and $p = 0$ outside the ellipsoid.

Figure 6 illustrates the obtained probability density curves. Figures 6(a) and 6(b) correspond to the steady state with the vertical component of diffusion and without it, respectively. Accordingly, Figs. 6(c) and 6(d) correspond to the perturbed state with the vertical component of diffusion and without it,

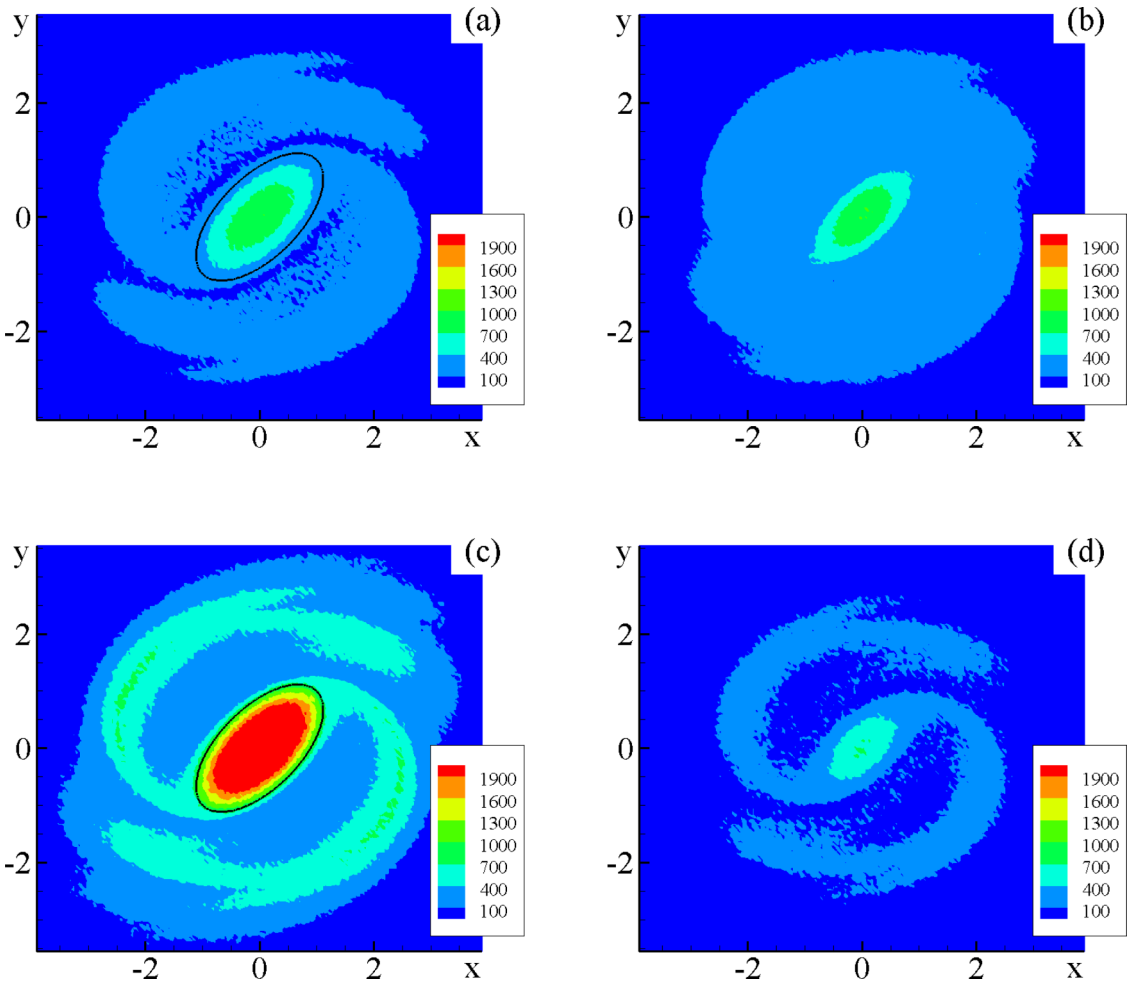

FIG. 5. (Color online) Perturbed state as $a(0)/b(0) = 2, \theta(0) = \pi/4$. Passive scalar distributions after 40 dimensionless time intervals from the initial concentration of 6×10^6 in each node as $\kappa = 0.01$. (a) $\kappa_z = 2\kappa$—the surface layer $z = 0$, the bold curve marks the steady ellipsoid boundary; (b) $\kappa_z = 2\kappa$—the layer comprising the bottom tip of the ellipsoid, $z = \tilde{c} = 1$; (c),(d) the same as in (a),(b), respectively, except that there is no vertical diffusion $\kappa_z = 0$.

respectively. Each figure comprises four curves corresponding to 10, 20, 30, and 40 time intervals. The steady-state figures are clearly indicative of a Gaussian distribution outside the ellipsoid, whereas the perturbed ones demonstrate different shapes.

In both steady and perturbed states, accounting for the vertical component of diffusion results in an intensification of the scalar transport out of the ellipsoid and saturation of the exterior region. In the perturbed case, concurrently with the diffusion there is chaotic advection that increases the flux through the ellipsoid boundary, resulting in a non-Gaussian distribution outside the ellipsoid within the chaotic advection region, which coincides roughly with the unperturbed separatrix region. In addition to the general intensification due to simple spreading of scalars in the vertical direction, the vertical component of diffusion also brings along the following feature. Since every cross section of the ellipsoid decreases in area with depth, a scalar starting in some horizon inside the ellipsoid can move to a deeper horizon but outside the ellipsoid, where it will be advected due to exponential divergence. This results in a decreased probability for the scalar to return inside the ellipsoid. This, in turn, enhances horizontal spreading. Figure 7(a), which shows the number of scalars inside the ellipsoid in time normalized by the total number of scalars, clearly demonstrates this effect. The curves corresponding to the cases with only horizontal diffusion components ($\kappa_z = 0$) are similar in the steady (the dashed lines) and perturbed states (the solid lines); the curves for the horizontal and vertical diffusion components are also similar, but they demonstrate more effective scalar spreading outside the ellipsoid. Figure 7(a) also features analogous curves figured out in the case $\kappa_z = \kappa$. The curves indicate that changing the vertical diffusivity results only in increased or decreased intensity of the fluid particles emanating from the ellipsoid, but no additional effects occur.

Another characteristic that can help to assess the structural deformation of the ellipsoid provided that scalars exchange with the exterior region is the dispersion of scalars originating from the ellipsoid. We use the term "dispersion" as a measure of passive scalar spreading in the directions of the ellipsoid's axes in space,

$$D_a = \langle x_a(t)^2 \rangle, \quad D_b = \langle y_b(t)^2 \rangle, \\ D_z = \langle z(t)^2 \rangle - \langle z(t) \rangle^2, \tag{10}$$

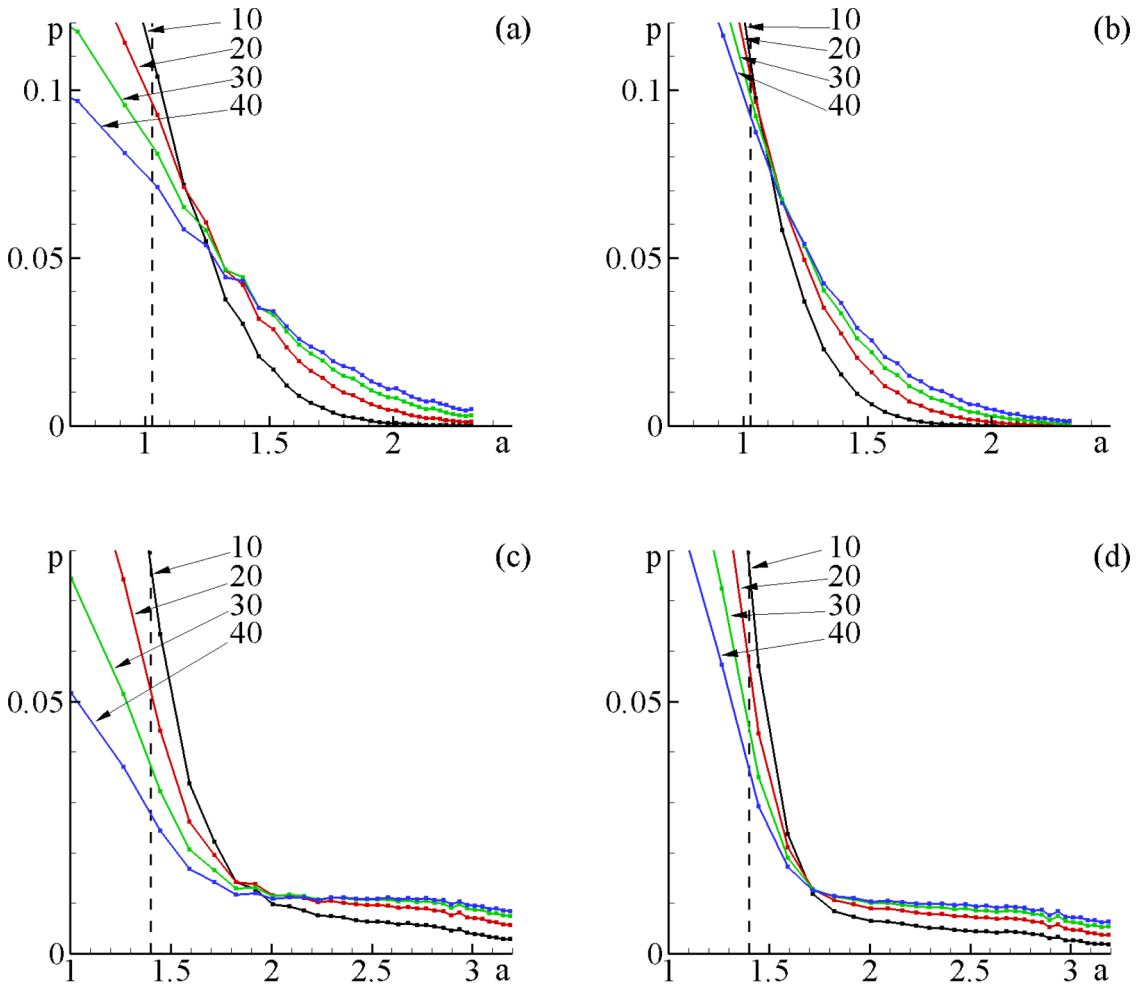

FIG. 6. (Color online) The probability density p as a function of the ellipsoid horizontal major axis a. Initially $p = 0.2$ inside the ellipsoid and $p = 0$ everywhere outside the ellipsoid. The vertical dashed line marks the boundary of the ellipsoid. Four curves in each part correspond to given dimensionless time intervals. (a) The steady state with the horizontal and vertical diffusion components, (b) the steady state with only the horizontal diffusion component, (c) the perturbed state with the horizontal and vertical diffusion components, and (d) the perturbed state with only the horizontal diffusion component.

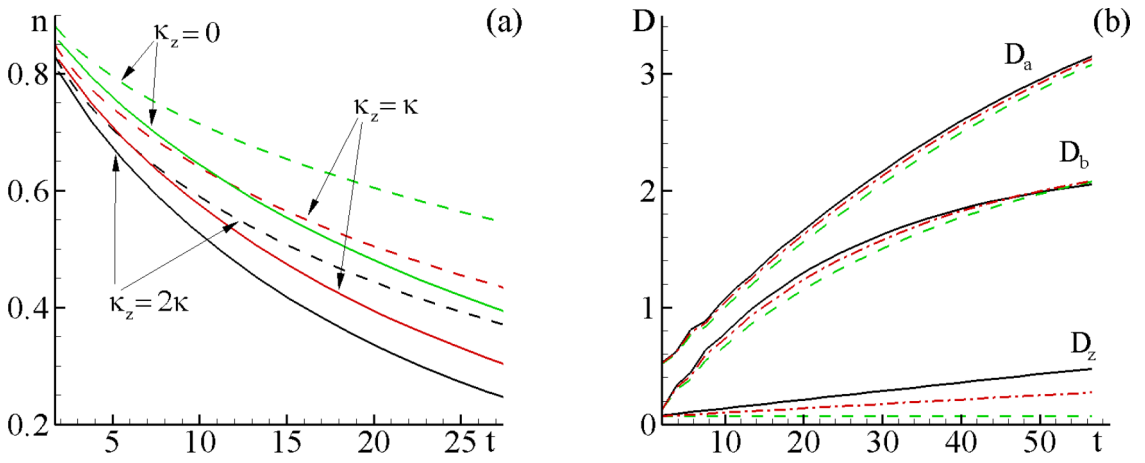

FIG. 7. (Color online) (a) The number of scalars inside the ellipsoid normalized by the total number of scalars depending on time. The dashed lines correspond to the steady states, while the solid lines correspond to the perturbed states. (b) Scalar dispersion components along the ellipsoid axes. The solid lines correspond to $\kappa_z = 2\kappa$, the dash-dotted lines correspond to $\kappa_z = \kappa$, and the dashed lines correspond to no diffusion vertical component $\kappa_z = 0$.

where $\langle\cdot\rangle$ is the averaging in the coordinate system bound to the ellipsoid horizontal axes, D_a, D_b are the dispersion components along the ellipsoid's horizontal axes, D_z is the dispersion component along the vertical axis, and x_a, y_b are the projections of a passive scalar position on the a and b axes, respectively.

In the steady state, which does not have exponential divergence of close trajectories, the dispersion components along the ellipsoid axes grow linearly in accordance with a Gaussian distribution, which is a solution of the stationary advection diffusion equation. Figure 7(b) illustrates the dispersion components along the ellipsoid axes in time. The steady-state case (not presented in the figure) corresponds to the linearly increasing lines complying with the equations

$$\begin{aligned} \langle x_a(t)^2\rangle = \langle y_b(t)^2\rangle = 4\kappa t, \\ \langle z(t)^2\rangle - \langle z(t)\rangle^2 = 4\kappa_z t. \end{aligned} \tag{11}$$

It is clear that Fig. 7(b) maintains these relations for the dispersion vertical component D_z in the perturbed state as the vertical motion is simply due to diffusion with no chaotic advection. Analogous linear dependencies are for all the dispersion components in the steady state. However, the dispersion horizontal components along the ellipsoid axes D_a and D_b behave differently, as can also be noticed from Figs. 6(c) and 6(d), which demonstrate apparent non-Gaussian distributions.

Opposite to the steady state, in the perturbed state the dispersion horizontal components have some features. First, the rate at which scalars emanate from the ellipsoid is considerably higher, and second, this rate decreases in time, indicating a nonlinear dependence. Accounting for the vertical diffusion component [the solid lines corresponding to the diffusivity $\kappa_z = 2\kappa$ and the dash-dotted lines corresponding to $\kappa_z = \kappa$ in Fig. 7(b)] results in a more distinct saturation effect. For example, after several tens of ellipsoid rotational periods, the dependences of the dispersion horizontal components cease to differ from the ones obtained with no diffusion vertical component. Based on these observations, we draw a conclusion that from the beginning, the ellipsoid breakup (in the sense of losing enough fluid particles from a region with different vorticity) is determined by advection of the scalars having been transported through the ellipsoid's boundary by diffusion. After the exterior region up to the separatrix region is properly saturated (distinguishing the closed recirculation region) further spreading of scalars into the exterior hyperbolic region is sustained by chaotic advection. The latter process occurs at rates distinctly slower than the former. Thus, scalars emanating from the ellipsoid swiftly spread within the separatrix region due to chaotic advection, but henceforth the rate at which scalars pass to the hyperbolic outer region will be significantly slower due merely to the diffusion process. In general, although the ellipsoid loses scalars, thus inducing its own breakup, these scalars stay for a significantly longer time within the separatrix region, decreasing the rate of decomposition of the whole rotational region, which comprises the ellipsoid and the surrounding closed recirculation region.

VI. CONCLUSIONS

In this paper, we have analyzed the passive scalar dynamics in an ellipsoid vortex model evolving in a linear shear flow subjected to diffusion. Despite being significantly refined, this model still provides valuable insights into the isolated vortex dynamics in the ocean [3,10]. With regard to the horizontal and vertical components of diffusion, we presented evidence that even though the vertical component of diffusion is several orders smaller than the horizontal component, it may be just as important and influential to the scalar transport in vortex structures in such sheared media.

Comparing the steady and perturbed states, i.e., those for which the ellipsoid stays still or those for which it rotates periodically, we have demonstrated that the vertical component of diffusion has a considerable effect on scalar distribution in the perturbed state. This is because, in the perturbed state, the diffusion vertical component can force a scalar to move between the ellipsoid's horizontal sections, which differ in area with depth. Therefore, there are events when scalars initially located in a regular dynamics horizontal section inside the ellipsoid find themselves in a lower section already outside the ellipsoid subjected to chaotic advection. Another noticeable effect is that, in both cases in the perturbed state, the horizontal dispersion component ratio D_a/D_b shown in Fig. 7(b), which was initially equal to 4, first decreases. This signifies that the closed recirculation region is being filled with scalars unevenly, and consequently the filled recirculation region shape becomes more circular. Furthermore, the dispersion ratio begins to increase, which means that the scalar patch shape again becomes more elliptical. The latter might be of interest since the scalar patch can be associated to some degree with vorticity inside coherent structures in geophysics. Thus the vorticity patch is redistributed unevenly resulting in a change in its ellipticity, which in turn affects the rate of decomposition of the vortex structure.

ACKNOWLEDGMENTS

The reported study was partially supported by the RFBR research projects: 14-05-00017, 15-05-00103, 15-35-20105; and by the FEBRAS project: 15-I-1-003 o. ER was partially supported by the Ministry of Education and Science of Russian Federation, project: MK-3084.2015.1.

[1] V. V. Zhmur, Localized eddy formation in a shear-flow, Oceanology **28**, 536 (1988).

[2] V. V. Zhmur, Subsurface mesoscale eddy structures in a stratificated ocean, Oceanology **29**, 28 (1989).

[3] S. P. Meacham, K. K. Pankratov, A. F. Shchepetkin, and V. V. Zhmur, The interaction of ellipsoidal vortices with background shear flows in a stratified fluid, Dyn. Atmos. Oceans **21**, 167 (1994).

[4] S. Kida, Motion of an elliptic vortex in a uniform shear flow, J. Phys. Soc. Jpn. **50**, 3517 (1981).

[5] S. P. Meacham, Quasigeostrophic, ellipsoidal vortices in stratified fluid, Dyn. Atmos. Oceans **16**, 189 (1992).

[6] H. Hashimoto, T. Shimonishi, and T. Miyazaki, Quasi-geostrophic ellipsoidal vortices in a two-dimensional strain field, J. Phys. Soc. Jpn. **68**, 3863 (1999).
[7] W. J. McKiver and D. G. Dritschel, The motion of a fluid ellipsoid in a general linear background flow, J. Fluid Mech. **474**, 147 (2003).
[8] D. G. Dritschel, J. N. Reinaud, and W. J. McKiver, The quasi-geostrophic ellipsoidal vortex model, J. Fluid Mech. **505**, 201 (2004).
[9] V. V. Zhmur, E. A. Ryzhov, and K. V. Koshel, Ellipsoidal vortex in a nonuniform flow: Dynamics and chaotic advections, J. Mar. Res. **69**, 435 (2011).
[10] W. J. McKiver, The ellipsoidal vortex: A novel approach to geophysical turbulence, Adv. Math. Phys. **2015**, 613683 (2015).
[11] H. Aref, Stirring by chaotic advection, J. Fluid Mech. **143**, 1 (1984).
[12] H. Aref, The development of chaotic advection, Phys. Fluids **14**, 1315 (2002).
[13] K. V. Koshel and S. V. Prants, Chaotic advection in the ocean, Phys.-Usp. **49**, 1151 (2006).
[14] L. M. Polvani and J. Wisdom, Chaotic Lagrangian trajectories around an elliptical vortex parch embedded in a constant and uniform background shear flow, Phys. Fluids A **2**, 123 (1990).
[15] L. M. Polvani, J. Wisdom, E. DeJong, and A. P. Ingersoll, Simple dynamical models of Neptune's Great Dark Spot, Science **249**, 1393 (1990).
[16] M. D. Dahleh, Exterior flow of the Kida ellipse, Phys. Fluids A **4**, 1979 (1992).
[17] M. G. Brown and R. M. Samelson, Particle motion in vorticity-conserving, two-dimensional incompressible flows, Phys. Fluids **6**, 2875 (1994).
[18] G. Haller and G. Yuan, Lagrangian coherent structures and mixing in two-dimensional turbulence, Physica D **147**, 352 (2000).
[19] S. Wiggins, The dynamical systems approach to Lagrangian transport in oceanic flows, Annu. Rev. Fluid Mech. **37**, 295 (2005).
[20] E. M. Bollt, A. Luttman, S. Kramer, and R. Basnayake, Measurable dynamics analysis of transport in the Gulf of Mexico during the oil spill, Int. J. Bifurcation Chaos **22**, 1230012 (2012).
[21] S. V. Prants, Dynamical systems theory methods to study mixing and transport in the ocean, Phys. Scr. **87**, 038115 (2013).
[22] B. N. Filyushkin, M. A. Sokolovskiy, N. G. Kozhelupova, and I. M. Vagina, Lagrangian methods for observation of intrathermocline eddies in ocean, Oceanology **54**, 688 (2014).
[23] G. Haller, Lagrangian coherent structures, Annu. Rev. Fluid Mech. **47**, 137 (2015).
[24] M. R. Allshouse and T. Peacock, Lagrangian based methods for coherent structure detection, Chaos **25**, 097617 (2015).
[25] K. V. Koshel, E. A. Ryzhov, and V. V. Zhmur, Diffusion-affected passive scalar transport in an ellipsoidal vortex in a shear flow, Nonlin. Processes Geophys. **20**, 437 (2013).
[26] V. Rom-Kedar and A. C. Poje, Universal properties of chaotic transport in the presence of diffusion, Phys. Fluids **11**, 2044 (1999).
[27] D. R. Lester, M. Rudman, G. Metcalfe, M. G. Trefry, A. Ord, and B. Hobbs, Scalar dispersion in a periodically reoriented potential flow: Acceleration via Lagrangian chaos, Phys. Rev. E **81**, 046319 (2010).
[28] K. Guseva, U. Feudel, and T. Tel, Influence of the history force on inertial particle advection: Gravitational effects and horizontal diffusion, Phys. Rev. E **88**, 042909 (2013).
[29] M. Giona, P. D. Anderson, and F. Garofalo, Short-time behavior of advecting-diffusing scalar fields in Stokes flows, Phys. Rev. E **87**, 063011 (2013).
[30] D. R. Lester, G. Metcalfe, and M. G. Trefry, Anomalous transport and chaotic advection in homogeneous porous media, Phys. Rev. E **90**, 063012 (2014).
[31] A. Okubo, Oceanic diffusion diagrams, Deep Sea Res. **18**, 789 (1971).
[32] A. S. Monin and R. V. Ozmidov, *Turbulence in the Ocean* (Reidel, Dordrecht, 1985), p. 247.
[33] A. Lichtenberg and M. Lieberman, *Regular and Stochastic Motion* (Springer-Verlag, New York, 1983).
[34] G. Zaslavsky, *Physics of Chaos in Hamiltonian Dynamics* (Imperial College Press, London, 1998).
[35] V. I. Klyatskin, Statistical description of the diffusion of a passive tracer in a random velocity field, Phys.-Usp. **37**, 501 (1994).
[36] K. V. Koshel and O. V. Alexandrova, Some results of a numerical modeling of the diffusion of passive tracers in a random field of velocities, Izv. Atmos. Ocean. Phys. **35**, 578 (1999).
[37] V. I. Klyatskin and K. V. Koshel, Simple example of the development of cluster structure of a passive tracer field in random flows, Phys.-Usp. **43**, 717 (2000).
[38] V. I. Klyatskin, *Stochastic Equations through the Eye of the Physicist (Basic Concepts, Exact Results, and Asymptotic Approximations)* (Elsevier, Science, 2005), p. 556.